Analyst

ARTICLE

Dual Amplification of Single Nucleotide Polymorphisms Detection Using Graphene Oxide and Nanoporous Gold Electrode Platform

Seyyed Mehdi khoshfetrat and Masoud A. Mehrgardi*

In the present manuscript, a strategy to prompt the sensitivity of the biosensor based on dual amplification of the signal by applying nanoporous gold electrode (NPGE) as the support platform and soluble graphene oxide (GO) as an indicator has been developed. By increasing the surface area of the biosensing platform and unique GO/ss-DNA interactions, the sensitivity for the detection of SNPs is enhanced. In the presence of SNPs, because of the less effective hybridization of mutant targets in compared to the complementary targets, further GO could adsorb on mutant targets-modified NPGE via $\pi-\pi$ interaction and cause a large increase of the charge transfer resistance (R_{ct}) of the electrode. This protocol provides a cost-effective and fast for discrimination of different SNPs. Furthermore, this biosensor can detect thermodynamically stable SNP (G-T mismatches) in the range of 15-1600 pM. The present strategy is a label-free and sensitive protocol and does not require sophisticated fabrication.

1. Introduction

Fast and simple determination of specific sequences of deoxyribonucleic acid (DNA) at low concentrations, particularly the methods for the rapid identification of base mutations or single nucleotide polymorphisms (SNPs), would prove useful in the diagnosis of many genetic diseases and in clinical, forensic and pharmaceutical application [1]. Electrochemical techniques can provide great advantages over the other existing devices due to their simplicity, rapidness, low-cost, high sensitivity and selectivity [2]. One of the key steps for the fabrication of DNA electrochemical biosensors is the amount and the stability of the immobilized single-stranded DNA (ss-DNA) probe as well as the accessibility of the target DNA toward the probe DNA immobilized electrode [3]. Therefore, increasing the immobilization amount and controlling over the molecular orientation of ss-DNA improve the performances of DNA biosensors [4]. So far, numerous different immobilization strategies have been reported and employed for increasing the amount of immobilized DNA. The introduction of nanomaterial could effectively increase the electrode surface area and enlarge the DNA immobilization amounts [5]. Cai et al. [6] assembled the AuNPs on a cysteamine-modified gold electrode and demonstrated that the immobilization quantities of thiolated probe DNA on the modified electrode are largely increased in compared to a bare gold electrode. Kelley research group [7] developed a strategy for the fabrication controlled nanowire and Pd nanostructures modified electrodes and achieved more

sensitive DNA detection through controlling the orientation of DNA probe. Hu and his co-workers [8] developed an electrochemical DNA biosensor based on nanoporous gold electrode and multifunctional encoded DNA–Au bio barcodes. Our research group recently reported a strategy for the detection of thermodynamically single base mismatches using nanoporous gold electrode (NPGE) [9]. NPGEs owing to prominent properties, such as high specific surface area, biocompatibility, excellent conductivity, chemical and thermal stability and toxicological safety are attractive platforms for the immobilization of biocomponents [10, 11]. Since, the methods for preparation of NPGEs, such as template-directed synthesis [12], hydrothermal treatment [13], electrochemical/chemical dealloying [14, 15], are usually involved in complex procedures, their applications for the signal amplification of DNA electrochemical biosensors are limited [16]. The construction of nanoporous modified electrodes by a simple strategy to achieve high sensitivity is extremely desirable. Recently, some new facile electrochemical strategies have been reported for the fabrication of NPGEs [17-20]. As nanostructured biointerface, in-situ prepared NPGEs are very appropriate for the construction of electrochemical biosensors due to their easy manipulation and high stability. Much more attentions have been focused on the sensitivity enhancement for the detection of DNA hybridization based on the avidin-hydrazine label [21], functionalized liposome [22], redox-active reporter molecule and enzyme label [23], metal/semiconductor nanoparticle label [24, 25].
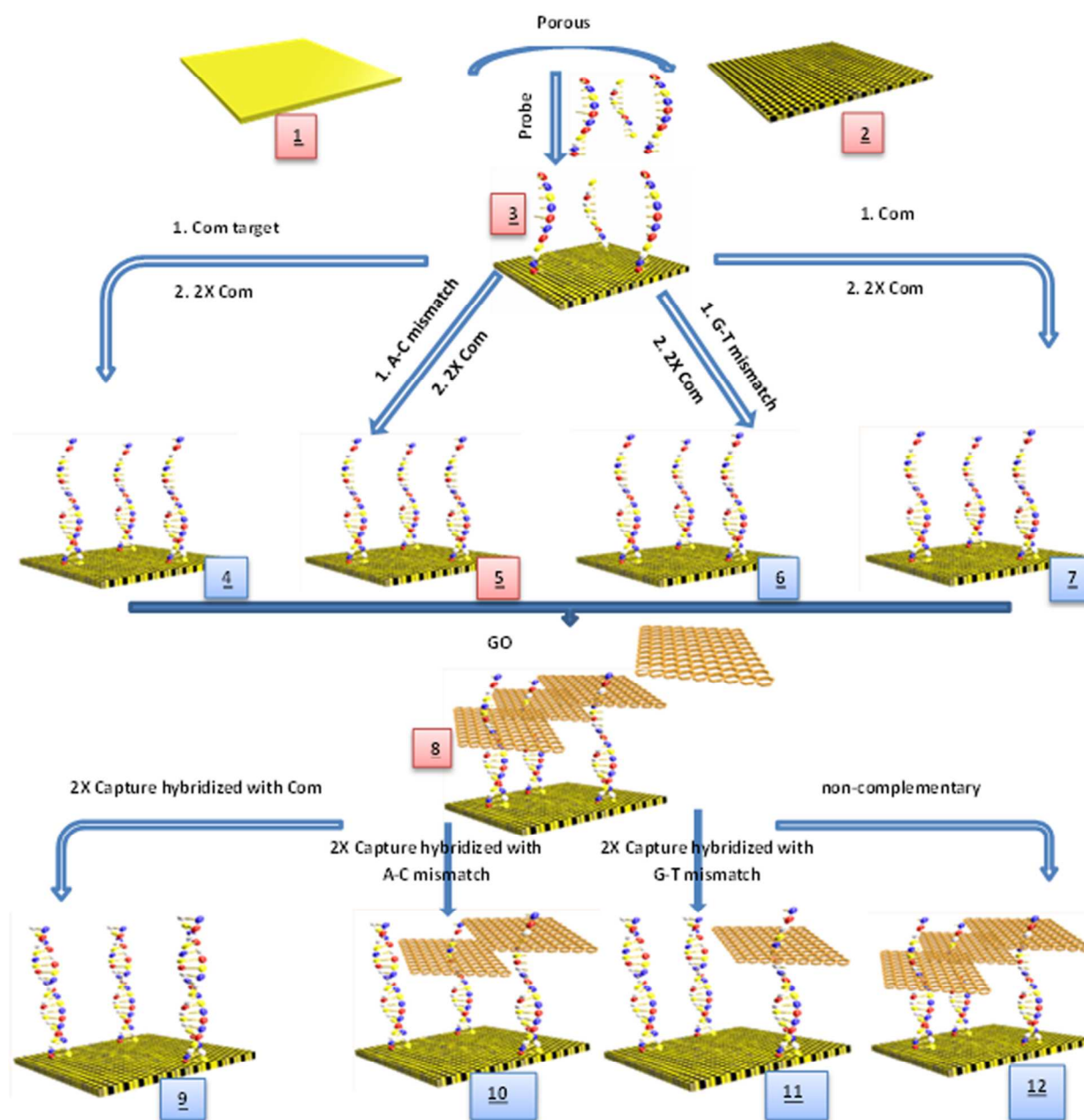
Scheme 1. Schematic presentation of different modification steps for fabrication Graphene Oxide-based Nanoporous Gold Electrode Platform.

While these methods generally have suitable detection limits, their practical application is restricted due to the complicated detection procedures (e.g., multiple redox cycling) or conjugation chemistries (e.g., labeling of enzymes and nanoparticles, etc.). It is still a major challenge to develop new technologies with improved simplicity, selectivity, and sensitivity of DNA hybridization detection that do not require complicated fabrication, instrumentation, and additional reagents.

Graphene Nanosheet (GN), single-layer carbon atoms densely packed into a two-dimensional honeycomb lattice, is the newest member of the carbon materials family [26-29]. GN because of its excellent electrical, mechanical, chemical and sensing performances [30-33], has been used in various electrochemical

applications. GN is a hydrophobic material and aggregate in the aqueous media [34, 35]. To improve its solubility in water, GN is oxidized to graphene oxide (GO) by generating surface carboxylic acid and hydroxyl groups. Recent studies have demonstrated that GN and GO can bind to single-stranded DNA (ss-DNA) via strong interactions, including van der Waals forces, π-π stacking, and/or hydrogen bond [36-41]. The unique GN or GO/ss-DNA interaction has shown fascinating applications including gene diagnosis, protein analysis, and intracellular tracking [42, 43]. However, exploration of this unique interaction in electrochemical biosensing is still at early stages. To the best of our knowledge, electrochemical detection of SNPs based on GO on NPGE platform has not been reported. In the present manuscript, the GO, as an insulating indicator of the

electrochemical signal, for the detection of SNPs is introduced. As it has been shown in Scheme 1, probe oligonucleotide was firstly immobilized on the NPGE surface via the Au−S chemistry. After hybridization with target and two times more concentrated complementary oligonucleotide (2X Com) to convert all single-strand probe DNA to double strand form, the un-hybridized part of target or Com oligonucleotide can strongly intercat with GO via the strong $\pi-\pi$ interaction and cause a large increase of the charge transfer resistance (R_{ct}), due to insulating property of GO and negatively charged backbone of DNA. However, the hybridization of the capture oligonucleotide would inhibit the GO interaction on the electrode; Therefore, R_{ct} was diminished, but the decrease for the mutant targets are less than Com target, because of less effective hybridization. Based on this strategy, a simple electrochemical DNA biosensor was fabricated for the sensitive detection of SNPs using GO on NPGE platform.

2. Materials and methods

2.1. Materials and reagents

The oligonucleotides used for this study were all obtained from Eurofins/MWG/Operon (Germany) with following sequences (5' to 3'): Probe: SH-$(CH_2)_6$- CTG CGT TTT; Capture: TTT TCG GCA; non-complementary: ACG AGC TAC; Target oligonucleotides includes: Complementary (Com): TGC CGA AAA AAA ACG CAG, A-C Mismatch: T**A**C CGA AAA AAA ACG CAG and G-T Mismatch: TGC **T**GA AAA AAA ACG CAG. The stock solutions of the oligonucleotides were prepared using PBS buffer solution (pH 7.4) containing 0.01 M Na_2HPO_4, 0.002 M KH_2PO_4, 0.15 M NaCl and 0.15 M KCl, and kept frozen at -20 ^{o}C. Tris(2-carboxyethyl)phosphine (TCEP), 6-mercaptohexanol (MCH), Sodium chloride, potassium chloride, magnesium chloride, sodium dihydrogen phosphate, disodium hydrogen phosphate, hydrochloric acid, nitric acid, sulfuric acid, potassium ferrocyanide and ferricyanide, ascorbic acid were purchased in analytical grade from commercial sources (Merck or Sigma).Triply distilled water was used throughout the experiments.

2.2. Instrumental

All electrochemical experiments were carried out using an Autolab PGSTAT30 (ECO Chemie, The Netherlands, driven by GPES4.9 software). The detection was performed in a home-made [44] electrochemical cell containing small parts of gold recordable compact disks (CDtrode) as the working electrode, an Ag/AgCl/3M KCl as a reference electrode and a platinum wire as an auxiliary electrode. The electrochemical impedance spectroscopy (EIS) and voltammetric measurements were performed in a solution containing $K_3[Fe(CN)_6]/K_4[Fe(CN)_6]$ (1:1, 0.5 mM) and KCl (0.1 M). The EIS measurements were performed by applying an AC potential with signal amplitude of 5 mV and frequency range over 10 kHz to 0.1 Hz, at the open circuit potential (OCP). Scanning electron microscopy (SEM) was accomplished on a PHILIPS XL–30 ESEM at an accelerating voltage of 20 KV. X-ray diffraction (XRD) patterns of the samples were recorded on a Bruker D8/Advance X-ray diffractometer with Cu-K_α radiation at 40 KV and 40 mA. The Absorbance measurements were performed using a JASCOV-670 UV–Vis. spectrophotometer. Thermogravimetric

analysis (TGA) of graphite and graphene oxide was carried out under N_2 flow using Thermogravimetric Analyzer Q50 (USA) and their masses were recorded as a function of temperature. The samples were heated from room temperature to 600 °C at 10°C/min. The FT-IR spectra were recorded using JASCO, FT/IR-6300 (Japan) and the surface Raman spectra were collected on a SENTERRA Raman spectrometer using 745 nm laser excitation.

2.3. Preparation of NPGE

A piece of a CD was cut down and the protective layer was removed by putting it in the concentrated nitric acid according to previously reported procedure [18, 45-47]. Then, it was washed with water thoroughly. Subsequently, the CDtrode was electrochemically cleaned with 0.01 M NaOH and 0.05 M H_2SO_4 **(1)**. The NPGE **(2)** was prepared in two steps according to previous methods [9, 18]. In the first step, the gold surface electrode was anodized by applying a step potential of 3.6 V in a phosphate buffer solution (pH 7.4) for 3 min. In the second step, the anodized gold surface was reduced to metallic Au for 5 min using of 1.0 M of ascorbic acid as a non-toxic and low-cost reducing agent. The color of the CDtrode surface changed to dark due to construction of nanoporous structure.

2.4. Preparation of GO

Graphene oxide (GO) was synthesized from natural graphite powder by a modified Hummer's method that has been previously reported by Shi et. al. [48]. Briefly, 3 g Graphite powder was put into 12 mL concentrated H_2SO_4 (80 °C), 2.5 g $K_2S_2O_8$, and 2.5 g P_2O_5 for 4.5 h. Then, the mixture was filtered and washed with DI water to remove the residual acid. The pretreated graphite powder was put into 120 mL cold (0 °C) concentrated H_2SO_4. Then, 15 g $KMnO_4$ was added gradually under stirring under 20 °C temperature. Then it was diluted to 700 mL. Subsequently, 20 mL of 30% H_2O_2 was added to the mixture. In this step, the color of mixture changed into brilliant yellow along with intensive releasing of the bubbles. The mixture was then filtered and washed with 1:10 HCl aqueous solution (~1 L) to remove metal ions followed by gently washing to remove the acid. Exfoliation was carried out by sonicating of 0.1 mg mL^{-1} GO dispersion under ambient condition for 30 min. The resulting homogeneous yellow-brown dispersion shows high stability over several months.

2.5. Modification of NPGE

The thiolated probe was freshly prepared, and disulfide bonds were reduced using TCEP solution. In a typical procedure, firstly, a 20 μL aliquot of the 6 μM probe with 4 μL of 0.5 mM TCEP was incubated in the dark for 1h and was subsequently dropped on the NPGE at room temperature for 16 h to self-assembled the probe on the NPGE through the Au-S chemistry. The Probe-modified electrode was then washed using 10 mM PBS (pH7.40) to remove non-specifically adsorbed probes on the surface. 10 μL aqueous solution of 5 μM MCH solution was put on the CDtrode surface to further eliminate the non-adsorbed DNA molecules. Subsequently, 12 μL of the different concentration of the target oligonucleotide along with 4 μL of 2 M magnesium chloride was draped on the MCH/Probe-modified electrode **(3)**. After washing this MCH/Probe/target NPGE (MCH/Probe/Com **(4)**, MCH/Probe/A-C mismatch **(5)** and MCH/Probe/G-T mismatch **(6)**), a drop containing 12 μL of

complementary target (12 μM, two-times more concentrated than the probe; 2X Com) was added to electrodes and wait for another 2 h to complete hybridization reactions. After that 12 μL of 0.1 mg/mL GO was dropped on the electrode surface for 1h (GO-treated target modified **(8)**). In the next step, a drop containing 12 μL of 12 μM capture (again two-times more concentrate than the probe; 2X capture), and 2 μL of 2 M magnesium chloride was placed on the NPGE surface. The control experimental was carried out with non-complementary oligonucleotide.

3. Results and discussion

3.1. Characterization of NPGE

High surface area NPGE has attracted great interests for their applications as biosensors. Compared with untreated gold electrode, the NPGEs possess a much higher surface areas and better electron transfers, which offer a great number of adsorption sites for DNA, proteins and enzymes [8, 9]. The surface area of the untreated gold electrode **(1)** and NPGE **(2)** were measured by following their cyclic voltammograms in 0.5 M sulfuric acid. By assuming a specific charge of 386 μC/cm for the reduction of one monolayer of gold oxide to metallic gold [49], the electroactive surface area of the **(1)** and **(2)** electrodes are obtained equal to 0.21 ± 0.03 cm^2 and 1.2 ± 0.20 cm^2, respectively. These values represent ~6 times increase in the active area of the electrode after converting it to nanoporous form. Fig. 1 shows SEM images of both **(1)** and **(2)** electrodes. The image of **(2)** surface reveals a nanoporous structure, while that of the **(1)** substrate shows a smooth with parallel data storage grooves structure.
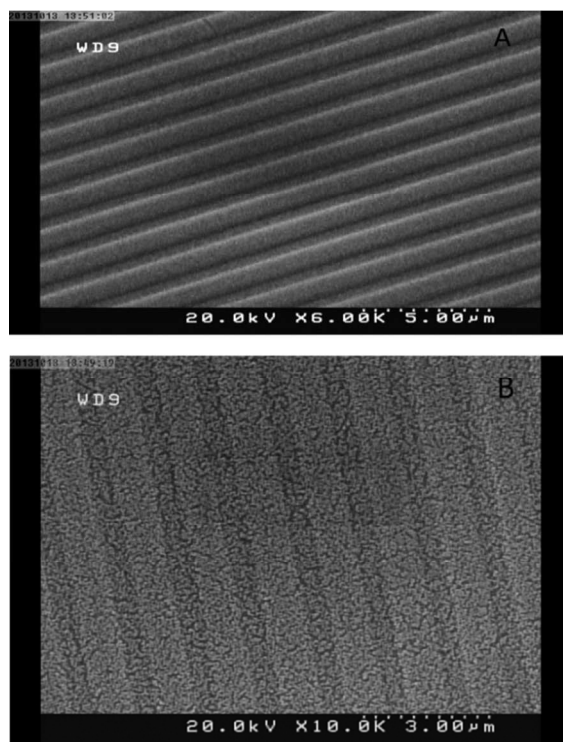
Fig. 1 SEM images of bare gold (A) and NPGE (B).

3.2. Characterization of GO

SEM image of GO (Fig. S1A) illustrates the exfoliated of GO was accomplished with formation of very thin layers flake-like structures. As shown in Fig. S1B, the feature diffraction peak of exfoliated GO appears at 11.4° (002) with inter-distance (d-spacing) of 7.75 A^o. This value is larger than the d-spacing (3.35 A^o) of pristine graphite (2θ=26.6°) due to the presence of oxygen containing functional groups [50]. The UV-Vis spectra (Fig. S1C) of yellow-brown of GO shows the distinct absorption peak at 230 nm due to π–π* transition of C=C bonds which is attributed to the characteristic absorption of GO [50, 51]. Fig. S2 shows FT-IR spectra of graphene oxide. The presence of different type of oxygen functionalities in graphene oxide was confirmed at 3400 cm^{-1} (O-H stretching vibrations), at 1720 cm^{-1} (stretching vibrations from C=O), at 1600 cm^{-1} (skeletal vibrations from unoxidized graphitic domains), at 1220 cm^{-1} (C-OH stretching vibrations), and at 1060 cm^{-1} (C-O stretching vibrations) [52]. The results of TGA are shown in Fig. S3. As expected, graphite was highly stable up to 600 °C. Graphene oxide shows a slight mass decrease from room temperature to 150 °C and significant decrease from 150 °C to 200 °C. The mass of graphene oxide slowly further decreased up to 600 °C. The major mass reduction at ~ 200 °C was caused by pyrolysis of the oxygen-containing functional groups, generating CO, CO_2 and stream [53]. As shown in Fig. S4 the Raman spectrum of GO displays two prominent peaks at 1600 and 1360 cm^{-1}, which correspond to the well-documented G and D bands [54].

3.3. The pH effect on interaction of GO with ss-DNA

To facilitate the interaction of GO with aromatic hydrophobic rings of DNA bases through π-π stacking, needs to overcome the electrostatic repulsion between DNA and negatively charged GO surface. Therfore, the control of surface charge of GO by changing the pH of the solution is a key parameter in the response of the biosensor. For this purpose, several PBS solutions with various pHs over the range of 4-8 were prepared. The adsorptions of GO on immobilized DNA strands on the electrode surface at various pHs were followed by incubation of MCH/Probe/Com electrode **(4)** for 1h at different pHs and recording the EIS spectra and voltammograms of the redox $[Fe(CN)_6]^{3-/4-}$ couple on the NPGE. Since, GO is an insulator, the charge transfer to the redox couple was expected to be more difficult after GO accumulation on the surface. As Fig. 2A and B show, the R_{ct} of EIS and peak separation of voltammograms for the redox couple increased significantly after exposure of the **(4)** to a GO solution at lower pHs. Based on these results, pH 4 was selected for detection as an optimum pH. The GO surface is terminated by several different the oxygen-containing group on its surface, and the pK$_a$ values of these groups should be close to that of benzoic acid (pK$_a$ = 4.2) or acetic acid (pK$_a$ = 4.7) [40, 55]. At neutral pH, these groups are deprotonated to give a highly negatively charged surface but at close to the pK$_a$'s, the surface charge is neutralized. The surface charge is neutralized to reduce repulsion; under these conditions, the π–π interactions or hydrophobic interactions dominate.

1
2
3
4
5
6
7
8
9
10
11
12
13
14
15
16
17
18
19
20
21
22
23
24
25
26
27
28
29
30
31
32
33
34
35
36
37
38
39
40
41
42
43
44
45
46
47
48
49
50
51
52
53
54
55
56
57
58
59
60
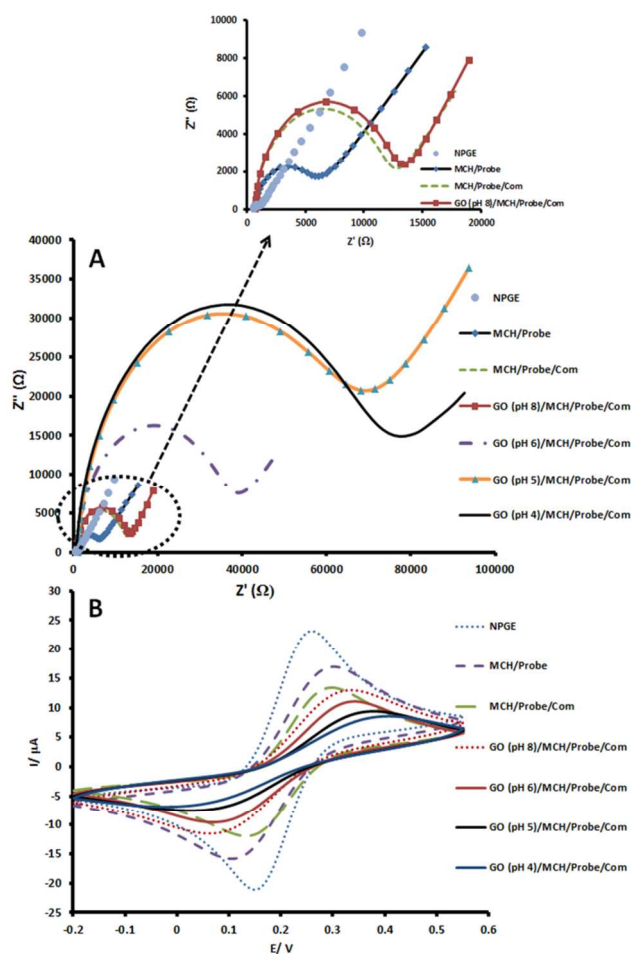
Fig. 2 Nyquist plots (A) and CVs (B) obtained for NPGE **(2)**, MCH/Probe **(3)**, MCH/Probe/Com **(4)** and GO-treated Com/NPGE **(5)** after exposing to different pH of GO solution.

3.4. Quantization of Surface Coverage of DNA immobilization

The surface coverage of the Probe-modified NPGE was determined by previously reported protocol by Steel et al [56]. Briefly, the chronocoulometric signals of the modified NPGE were followed in the presence and absence of a cationic redox reporter, ruthenium hexamine trichloride (RuHex), that are electrostatically bind to the negatively charged DNA backbone. After the immobilization of the probe on the electrode surface, the Probe-modified electrode was subjected in RuHex. Then, the amount RuHex, was measured by chronocoulometry using Cottrell equation. DNA surface density was then obtained using the following equation:

$$\Gamma_{DNA} = \Gamma_0 \left(\frac{z}{m}\right) N_A$$

Where Γ_{DNA} is the probe surface density in molecules/cm^2, m is the number of bases in probe DNA, z is the charge of RuHex and N_A is Avogadro's number. The surface density of probe DNA has been obtained equal to 5.2 ($\pm$0. 5) $\times 10^{12}$ molecules/cm^2.

3.5. Electrochemical detection of SNPs on NPGE

This assay has been designed for discrimination between various SNPs based on less effective hybridization of mismatch targets in compared to complementary target and the differences between interaction of GO sheets with ss-DNA and ds-DNA. Therefore, if whole DNA probe strands on the electrode surface are not hybridized with their complementary bases, GO can interact with their free bases. To avoid this problem, after addition of different concentrations of targets, 2X Com was dropped on the electrode surface. It is worthy to mention that the lower section of complementary and mismatch targets are completely the same and complementary with the probe sequence. Fig. 3 (spectrum a) shows the EIS, using $Fe(CN)_6^{3-}/Fe(CN)_6^{4-}$ as redox probe on the surface of MCH/Probe/NPGE **(3)**. Upon hybridizing of the probe with mismatch or complementary targets following by treating by excess complementary target (2X com) the negative charges on the surface are developed **(4** or **5** or **6)** and R$_{ct}$ is increased (Spectrum b). Since the hybridizing segment of different targets with probe is the same, therefore no significant differences in EIS were not observed on the surface of **4**, **5** or **6**.
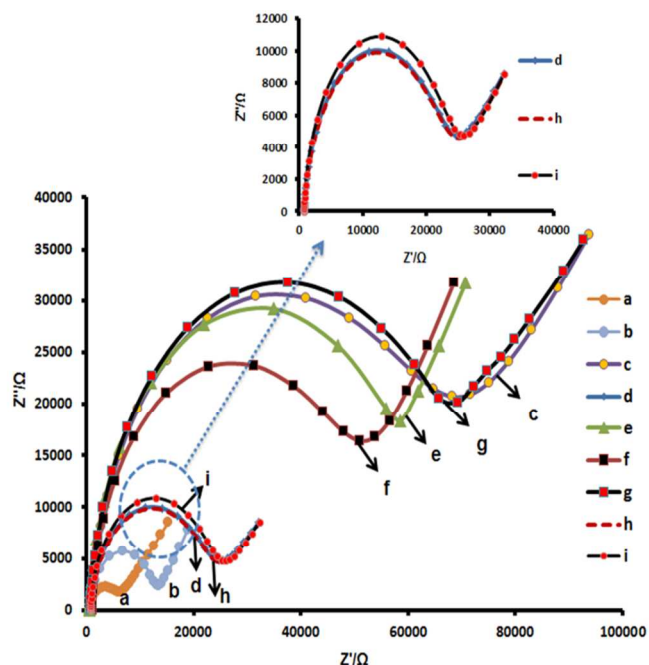
Fig. 3 Nyquist plots recorded on the electrode surface **(3)** (a), MCH/Probe/target **(4, 5, 6)** (b), GO-treated targets **(8)** (c), capture hybridized with Com target **(9)** (d), with A-C mismatch **(10)** (e), with G-T mismatch **(11)** (f) and negative control with a non-complementary sequence **(12)** (g). MCH/Probe/Com **(4)** after treatment of capture without GO (h). MCH/Probe/Com **(4)** first reacted with capture oligonucleotide and then incubated with 0.1 mg/mL GO for 1 h (i).

By treating the MCH/Probe/target NPGE surface with GO sheets, they strongly interact with non-hybridized moiety of targets via π-π interactions **(8)** and cause dramatically increase in R$_{ct}$ due to the hindrance introduced by the adsorption of the insulating GO on the electrode surface (spectrum c). In the next step, by hybridization of capture oligonucleotide with a non-hybridized section of the Com **(9)**, A-C **(10)** or G-T mismatch **(11)**, charge transfer resistances have

been decreased (spectra of d, e and f respectively), while the treatment of the surface with non-complementary target does not change R_{ct} significantly (spectrum (g)).

The treatment of complementary target with 2X capture **(9)** shows the most decrease in the resistance (spectrum d). This R_{ct} is as similar as the resistance observed for the same surface, but without treating with GO sheets (spectrum h). It's demonstrating, for the Com targets, the hybridization is approximately complete and all of GO sheets leave the surface. Also the hybridization of Com target with 2X capture followed by treating with GO sheets does not change the R_{ct} significantly (spectrum i). It is another evidence demonstrating no interaction between ds-DNA and GO and also no nonspecific adsorption of GO on ss-DNA Probe, as well. On the other side, the R_{ct} for A-C and G-T mismatch targets **(10 and 11)** is also decreased by treating of the surface with 2X capture, but not as large as decrease in R_{ct} of the Com target (spectra e and f) that can be attributed to less effective hybridization of mismatch targets. Another worthy point that observed here, is the difference between R_{ct} of A-C **(10)** and G-T mismatches **(11)** (spectra e and f). The G-T mismatch is thermodynamically more stable than A-C mismatch. Therefore, the hybridization of G-T mismatches is more effective than A-C mismatches and less effective than complementary targets. Therefore, the remaining GO on the surface would be more than Com targets and less than A-C mismatch targets. It causes larger R_{ct} in compared to Com targets (spectrum d) and smaller R_{ct} in compared to A-C mismatch targets (spectrum f). Finally, for non-complementary targets **(12)** no significant changes in R_{ct} (spectrum g) are observed in compared to the surface **(8)**.

As Fig. 4 shows, when the concentration of G-T mismatches is increased, the R_{ct} is increased as well. It can be attributed to less effective hybridization G-T mismatches in compared to Com targets, which causes more interaction of insulating GO with non-hybridized section of G-T mismatches and gradually increase in the R_{ct}. There is a logarithmic relationship between R_{ct} and the G-T mismatch concentrations over a range from 15 pM to 1600 pM (Inset Fig. 4). Therefore, the presented method could be successfully applied for the detection and quantification of different SNPs in their low concentration levels.
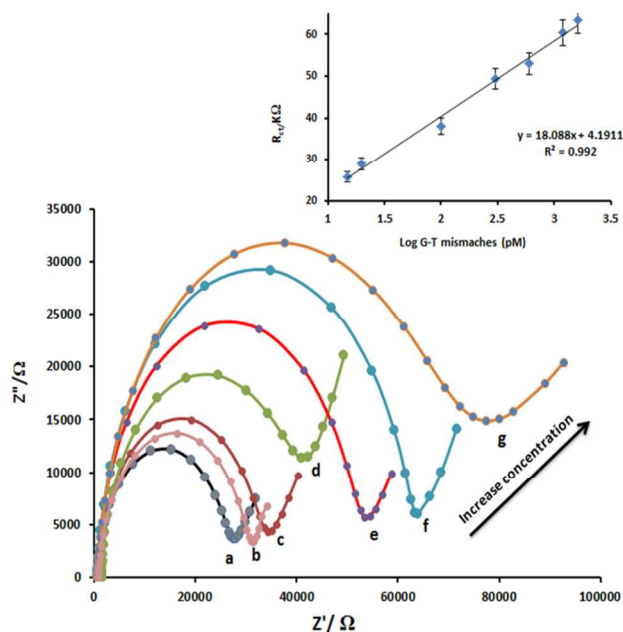
Fig. 4 Nyquist plots for EIS detection of various concentrations (a: 15; b: 20; c: 100; d: 300; e: 600; f: 1200; g: 1600 (pM)) of thermodynamically stable G-T mismatches on GO-treated G-T mismatches **(11)**. (Inset) the resulting calibration curve.

At the last not the least, to demonstrate that decreases in the resistances is only originated by the hybridization process and not by for example instability of GO sheets on the surface, their stabilities were checked by recording 50 cyclic voltammograms on the GO-treated Com **(8)**. Fig. 5 demonstrates that GO sheets on the surface **(4)** is very stable, which shows the almost changeless redox peak currents of $[Fe(CN)_6]^{3-/4-}$.
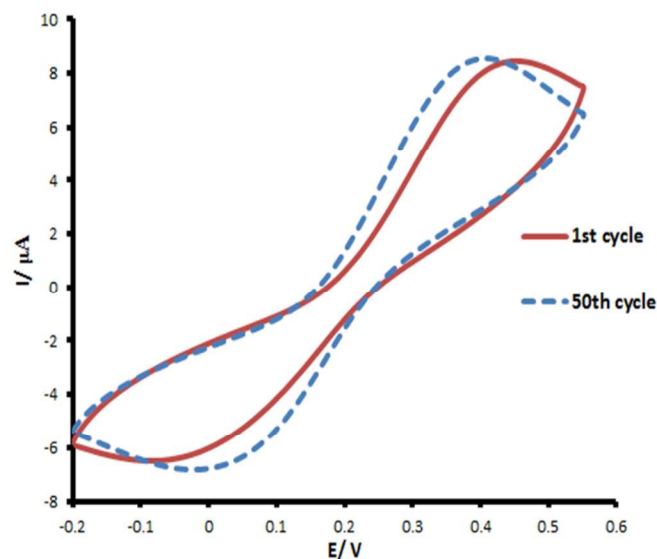
Fig. 5. Stability of GO-treated Com NPGE (**8**) after 50 cycles.

4. Conclusion

Efficient, simple and highly sensitive electrochemical DNA biosensor by taking advantage of the NPGE, soluble graphene oxide (GO), and the unique GO/ss-DNA interaction for the detection of DNA hybridization and polymorphism using EIS have been developed. On the basis of differences between interaction of ss-DNA and dsDNA with GO, have been successfully detected different SNPs including, thermodynamically stable G-T mismatch, with a dynamic range of 15-1600 pM. The GO-based electrochemical biosensing NPGE platform has obvious advantages over the conventional method. First, NPGE provided high loading immobilized platform. Second, by combining of the soluble insulation of GO and the unique GO/ss-DNA interaction, a label-free detection strategy is realized, which makes the sensing process quite simple and convenient. Finally, since GO can be prepared from low cost graphite, the GO-based method is cost-effective.

Acknowledgement

Notes and references

[a] Department of chemistry, University of Isfahan, Isfahan 81746-73441, Iran. +98 3117932710; fax: +98 3116689732.

m.mehrgardi@chem.ui.ac.ir, m.mehrgardi@gmail.com (M.A. Mehrgardi)

References:

1. R. Salari, C. Kimchi-Sarfaty, M. M. Gottesman and T. M. Przytycka, *Nucleic Acids Res.*, 2013, **41**, 44-53.
2. G. Liu, T. M. Lee and J. Wang, *J. Am. Chem. Soc.*, 2005, **127**, 38-39.
3. K. B. Cederquist, R. Stoermer Golightly and C. D. Keating, *Langmuir*, 2008, **24**, 9162-9171.
4. T. H. Kjällman, H. Peng, C. Soeller and J. Travas-Sejdic, *Anal. Chem.*, 2008, **80**, 9460-9466.
5. F. P. Zamborini, L. Bao and R. Dasari, *Anal. Chem.*, 2011, **84**, 541-576.
6. H. Cai, C. Xu, P. He and Y. Fang, *J. Electroanal. Chem.*, 2001, **510**, 78-85.
7. L. Soleymani, Z. Fang, E. H. Sargent and S. O. Kelley, *Nature Nanotechnol.*, 2009, **4**, 844-848.
8. K. Hu, D. Lan, X. Li and S. Zhang, *Anal. Chem.*, 2008, **80**, 9124-9130.
9. L. E. Ahangar and M. A. Mehrgardi, *Biosens. Bioelectron.*, 2012, **38**, 252-257.
10. H. Qiu, L. Xue, G. Ji, G. Zhou, X. Huang, Y. Qu and P. Gao, *Biosens. Bioelectron.*, 2009, **24**, 3014-3018.
11. H. Qiu, C. Xu, X. Huang, Y. Ding, Y. Qu and P. Gao, *J. Phys. Chem. C*, 2009, **113**, 2521-2525.
12. H. Qiu, Y. Li, G. Ji, G. Zhou, X. Huang, Y. Qu and P. Gao, *Bioresour. Technol.*, 2009, **100**, 3837-3842.
13. A. Huczko, *Appl. Phys. A*, 2000, **70**, 365-376.
14. Q. Yi and W. Yu, *J. Electroanal. Chem.*, 2009, **633**, 159-164.
15. J. F. Huang and I. W. Sun, *Adv. Funct. Mater.*, 2005, **15**, 989-994.
16. F. Li, X. Han and S. Liu, *Biosens. Bioelectron.*, 2011, **26**, 2619-2625.
17. W. Huang, M. Wang, J. Zheng and Z. Li, *J. Phys. Chem. C*, 2009, **113**, 1800-1805.
18. A. Kiani and E. N. Fard, *Electrochim. Acta*, 2009, **54**, 7254-7259.
19. H. Qiu and X. Huang, *J. Electroanal. Chem.*, 2010, **643**, 39-45.
20. L. Kashefi-Kheyrabadi and M. A. Mehrgardi, *Bioelectrochemistry*, 2013, **94**, 47-52.
21. M. J. Shiddiky, M. A. Rahman, C. S. Cheol and Y.-B. Shim, *Anal. Biochem.*, 2008, **379**, 170-175.
22. F. Patolsky, A. Lichtenstein and I. Willner, *Angew. Chem. Int. Ed.*, 2000, **39**, 940-943.
23. S. Liu, P. Wu, W. Li, H. Zhang and C. Cai, *Anal. Chem.*, 2011, **83**, 4752-4758.
24. T. Selvaraju, J. Das, K. Jo, K. Kwon, C.-H. Huh, T. K. Kim and H. Yang, *Langmuir*, 2008, **24**, 9883-9888.
25. J. A. Hansen, R. Mukhopadhyay, J. Ø. Hansen and K. V. Gothelf, *J. Am. Chem. Soc.*, 2006, **128**, 3860-3861.
26. F. Kim, L. J. Cote and J. Huang, *Adv. Mater.*, 2010, **22**, 1954-1958.
27. C. e. N. e. R. Rao, A. e. K. Sood, K. e. S. Subrahmanyam and A. Govindaraj, *Angew. Chem. Int. Ed.*, 2009, **48**, 7752-7777.
28. A. K. Geim and K. S. Novoselov, *Nature Mater.*, 2007, **6**, 183-191.
29. S. Guo, D. Wen, Y. Zhai, S. Dong and E. Wang, *ACS Nano*, 2010, **4**, 3959-3968.
30. M. J. Allen, V. C. Tung and R. B. Kaner, *Chem. Rev.*, 2009, **110**, 132-145.
31. D. R. Dreyer, S. Park, C. W. Bielawski and R. S. Ruoff, *Chem. Soc. Rev.*, 2010, **39**, 228-240.
32. D. Chen, L. Tang and J. Li, *Chem. Soc. Rev.*, 2010, **39**, 3157-3180.
33. Y. Wang, Y. Shao, D. W. Matson, J. Li and Y. Lin, *ACS Nano*, 2010, **4**, 1790-1798.
34. H. Bai, Y. Xu, L. Zhao, C. Li and G. Shi, *Chem. Commun.*, 2009, 1667-1669.
35. J. Long, M. Fang and G. Chen, *J. Mater. Chem.*, 2011, **21**, 10421-10425.
36. N. Varghese, U. Mogera, A. Govindaraj, A. Das, P. K. Maiti, A. K. Sood and C. Rao, *ChemPhysChem*, 2009, **10**, 206-210.
37. C. H. Lu, H. H. Yang, C. L. Zhu, X. Chen and G. N. Chen, *Angew. Chem.*, 2009, **121**, 4879-4881.
38. Y. Wang, Z. Li, D. Hu, C.-T. Lin, J. Li and Y. Lin, *J. Am. Chem. Soc.*, 2010, **132**, 9274-9276.
39. L. Wang, M. Xu, L. Han, M. Zhou, C. Zhu and S. Dong, *Anal. Chem.*, 2012, **84**, 7301-7307.
40. H. Park, S.-J. Hwang and K. Kim, *Electrochem. Commun.*, 2012.
41. L. Tang, Y. Wang, Y. Liu and J. Li, *ACS Nano*, 2011, **5**, 3817-3822.
42. B. Gulbakan, E. Yasun, M. I. Shukoor, Z. Zhu, M. You, X. Tan, H. Sanchez, D. H. Powell, H. Dai and W. Tan, *J. Am. Chem. Soc.*, 2010, **132**, 17408-17410.
43. A. Bonanni and M. Pumera, *ACS nano*, 2011, **5**, 2356-2361.
44. L. E. Ahangar and M. A. Mehrgardi, *Electrochim. Acta*, 2011, **56**, 10264-10269.
45. L. Angnes, E. M. Richter, M. A. Augelli and G. H. Kume, *Anal. Chem.*, 2000, **72**, 5503-5506.
46. M. A. Mehrgardi and L. E. Ahangar, *Biosens. Bioelectron.*, 2011, **26**, 4308-4313.
47. M. A. Mehrgardi, *ChemElectroChem*, 2014, **1**, 779-786.
48. Y. Xu, H. Bai, G. Lu, C. Li and G. Shi, *J. Am. Chem. Soc.*, 2008, **130**, 5856-5857.
49. R. Szamocki, A. Velichko, C. Holzapfel, F. Mücklich, S. Ravaine, P. Garrigue, N. Sojic, R. Hempelmann and A. Kuhn, *Anal. Chem.*, 2007, **79**, 533-539.
50. H.-L. Guo, X.-F. Wang, Q.-Y. Qian, F.-B. Wang and X.-H. Xia, *ACS nano*, 2009, **3**, 2653-2659.
51. D. Li, M. B. Müller, S. Gilje, R. B. Kaner and G. G. Wallace, *Nature nanotechnology*, 2008, **3**, 101-105.
52. E.-Y. Choi, T. H. Han, J. Hong, J. E. Kim, S. H. Lee, H. W. Kim and S. O. Kim, *Journal of Materials Chemistry*, 2010, **20**, 1907-1912.
53. S. Stankovich, D. A. Dikin, R. D. Piner, K. A. Kohlhaas, A. Kleinhammes, Y. Jia, Y. Wu, S. T. Nguyen and R. S. Ruoff, *Carbon*, 2007, **45**, 1558-1565.

54. D. Graf, F. Molitor, K. Ensslin, C. Stampfer, A. Jungen, C. Hierold and L. Wirtz, *Nano letters*, 2007, **7**, 238-242.

55. Y. Miyake, H. Togashi, M. Tashiro, H. Yamaguchi, S. Oda, M. Kudo, Y. Tanaka, Y. Kondo, R. Sawa and T. Fujimoto, *Journal of the American Chemical Society*, 2006, **128**, 2172-2173.

56. A. B. Steel, T. M. Herne and M. J. Tarlov, *Anal. Chem.*, 1998, **70**, 4670-4677.